CHAPTER 5

SPECTROSCOPY SIGNAL PROCESSING IN CARDIAC DIAGNOSIS

Highlights of the Chapter

- *Application of spectroscopic methods were explored for detection of cardiac biomarker.*
- *UV-Vis spectroscopy provided the active and passive detection of cardiac biomarker.*
- *Application of Double density dual tree complex wavelet transform is evaluated for denoising and spike removal from spectroscopy signals.*

Abstract:

Disease-specific biomarker detection helps in determining the disease, taking preventive measures, and monitoring any physio pathological condition. Recently, advancement in optical and detection system increased the application of optical methods in medical diagnosis. UV-Visible and FTIR spectroscopy are optical methods that can be effectively used for quantitative analysis of biomarkers. However, noise, on the other hand, is inherent in any measurement and high signal to noise ratio is required for any signal analysis processing. In Raman spectroscopy, neglecting noise and spikes will influence further analysis and may lead to a false true or true false classification of the sample. This leads to the need for additional pre-processing step, spike-removal and denoising, before further analysis of spectrum. Several denoising methods have already been proposed among which Savitsky-Golay smoothing is most commonly used for the Raman signal. In many cases, the drawbacks of this smoothing method are observed. Here, we propose to use gold nanoparticles for surface plasmon generation and then conjugate cTnI to the nanoparticles. Conjugation of cTnI

showed complete quenching of the SPR of gold nanoparticles and a peak at around 200 nm in UV-Visible spectra and Peak transmittance variation in FTIR spectra. The study suggests that UV-Visible spectrophotometry is able to detect cTnI of as low as 2ng/μL concentration. Also, we aim to show the effectiveness of Double Density dual-tree complex wavelet transform to denoise the Raman signal. A comparative study is carried out to show the ability of Double Density dual-tree complex wavelet transform with Discrete wavelet transform, Dual tree complex wavelet transform and Savitsky-Golay smoothing method to show its effectiveness. Results show that Double Density dual-tree complex wavelet transform based denoising can improve quantitative and qualitative analysis of the Raman signal.

5.1 Introduction

5.1.1 Cardiac biomarker detection

Biomarkers are the biochemical component that is measured and evaluated in the situation of any physiological, pathological, or therapeutic process[1]. The concentration of the biochemical components defines the status of the body. Disease-specific biomarker detection helps in determining the disease, taking preventive measures, and monitoring any physio pathological condition. Any biomarker to be ideal for detection of physio-pathological condition should have properties like absence in other tissues (Specificity), rapid release in case of any abnormalities, concentration released proportional to damage, presence in plasma for diagnostic window, and suitable to analyze. Use of biomarkers for detection of cardiac injury started way back. In 1954, La Due used aspartate aminotransferase for acute myocardial infarction. Later, Creatine kinase and lactate dehydrogenase were reported as marker for cardiac abnormality. Cardiac Troponins (I and T)[3,4], C-reactive protein (CRP)[5], Tumor necrosis factor-alpha (TNF- α), Myoglobin[6], and

BNP/NT-proBNP are recently developed cardiac biomarker and generally used for cardiac health monitoring and diagnosis.

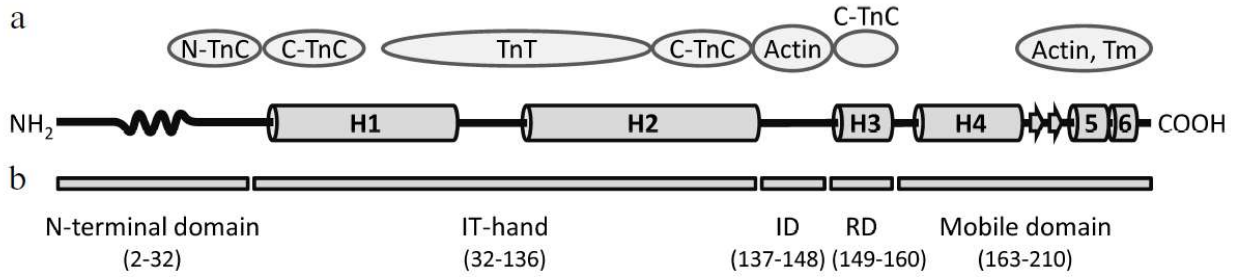

Figure 5.1: Cardiac Troponin I structure and its interactive surroundings

Cardiac troponin I is a protein subunit that inhibits muscle contraction in absence of calcium. It is a 24 kDa molecule that binds to Troponin C, Troponin T, and actin. The structural changes in Troponin C are transmitted to the troponin I after which it releases its inhibitory binding to actin in the on state when calcium is present. cTnI is established as a specific biomarker for detection of myocardial infarction, risk stratification of patients, and diagnosis of cardiac injury. Quick diagnosis and medical intervention play an important role in management of cardiac patients of high risk. In recent years, several biosensors had been developed by different research groups to quantify cardiac biomarkers. Electrochemical, Surface plasmon resonance, Field effect transistor-based techniques had been employed to develop detection systems. Although these methods are regarded as gold standard, several limitations still exist in the detection systems such as sample preparation, lack of inter-laboratory standardization, and time required to obtain results. Several biosensors were developed in recent years for fast and effective detection of cTnI. It is also often observed that patients with symptoms of the onset of cardiac event hesitate to report to the healthcare facility immediately with a delay of 4-hour median. This leads to a higher concentration of biomarkers suggesting prolonged ischemia and irreversible cardiac damage.

Prompt diagnosis and medical intervention are of utmost importance to minimize the threat of permanent damage or death.

Recently, several optical methods of qualitative and quantitative analysis of biomarkers had been developed. Raman spectroscopy, FTIR, SPR, Fluorescence, and UV-Visible spectroscopy are most used optical methods. Ultraviolet-visible spectroscopy or spectrophotometry (UV-Vis) refers to absorption spectroscopy in the ultraviolet-visible range. UV-Visible spectrophotometer is a non-destructive optical method used for quantitative analysis of the sample. The Beer-Lambert law states that the absorbance of a solution is directly proportional to concentration of the absorbing species in the solution and path length. Thus, if path length is fixed, absorbance changes with variation in concentration of target. FTIR on the other hand, is another optical technique to obtain an infrared spectrum of absorption or emission of a solid, liquid, or gas. The spectrum is in fact obtained by Fourier transform of raw data to obtain actual spectrum.

5.1.2 Spectroscopy signal processing

Charge-coupled devices (CCD) are used in most of dispersive Raman spectrometer because of benefits like high quantum efficiency, good sensitivity, high dynamic range and reliability and small thermal noise[7,8]. But CCD detectors are sensitive to cosmic rays leading to large sharp spikes in the spectra [9,10]. Spikes are randomly distributed in time and space making it difficult to remove. The presence of such spurious spikes may introduce a deleterious effect in further analysis of the signal. Thus, it is required to automatically identify and remove spikes from the spectra.

Techniques so far reported in the literature for removal of spike can be categorized as (i) Additional acquisition-based method (ii) Hardware-based methods (iii) Software-based methods.

In the additional acquisition-based method, it is assumed that the probability of occurrence of the cosmic spike at the same pixel in successive measurement is low. The hardware-based method includes methods such as analyzing the full CCD image, image curvature correction, and division of spectrograph slit. But this technique makes the system complex and costly [11]. Thus, software-based spike removal techniques are generally used for Raman spectra.

Signals are inherently corrupted by noise but are neglected because of the high signal to noise ratio (SNR). In Raman spectroscopy, neglecting the noise will influence further analysis and may introduce incorrect information and classification of the sample [12–14]. Raman spectra can be corrupted by various types of noises like dark current noise, analog to digital converter (ADC) noise, fluorescence background, and random noises. Among these, noise due to fluorescence background and random noise is dominant. Only Random noise is considered here.

Denoising has been a major challenge in signal pre-processing. Several denoising methods have already been proposed among which polynomial least-squares smoothing filter, also known as Savitsky-Golay smoothing, is most commonly used for the Raman signal [15]. It dynamically fits polynomial to consecutive windows of signal to follow the shape of the randomly varying signal. In many cases, the drawback of this smoothing method is observed. If the frame length of the window is small, the denoised signal will remain noisy, and if the frame length of the window is large, the spectral resolution will be poor and causes distortion in spectral features.

Denoising using transforms (domain change) is an alternative to remove noise. Ethrentreich et al compared denoising capability of Wavelet transform and Fourier transform and concluded that wavelet transform performs better [16]. Also, Wentzell et al in 2000 used FIR filters, IIR filters, and Kalman filters as an alternative to denoise Raman spectra [17]. Greek et al in 1995 and Craggs et al in 1996 used maximum entropy methods for signal recovery but it requires

multivariate equation solving which is computationally expensive and the problem of convergence was reported [18,19].

In this chapter, we propose to use gold nanoparticles surface plasmon as detection tool. Gold nanoparticles is established to show surface plasmon at approx. 530 nm for size of 10 nm and when gold nanoparticles are conjugated with bigger molecule, SPR peak generally red shifts. The cTnI conjugation in this study with gold nanoparticles instead of shifting quenched the SPR. Also, we aim to show the effectiveness of Double Density dual-tree complex wavelet transform to denoise the Raman signal. A comparative study is carried out to show the ability of Double Density dual-tree complex wavelet transform with Discrete wavelet transform, Dual tree complex wavelet transform and Savitsky-Golay smoothing method to show its effectiveness. Results show that Double Density dual-tree complex wavelet transform based denoising can improve quantitative and qualitative analysis of the Raman signal.

5.2 Materials and Methods

Gold chloride, lithium borohydride, N-(3-dimethyl)-N-ethyl carbodiimide hydrochloride (EDC) and N-hydroxy sulfo succinimide (NHS) were purchased from Sigma-Aldrich. All other reagents used were of analytical grade and experiments were performed using Milli-Q (8.2 MΩ). Recombinant Human cTnI was purchased from ProSpec-Tany TechnoGene Ltd, Israel which was produced in E.Coli is a single, non-glycosylated polypeptide chain containing 210 amino acids and having a molecular mass of 24 kDa. cTnI was purified by chromatographic techniques with purity greater than 95.0%.

Gold nanoparticle synthesis: Gold nanoparticles (AuNPs) were prepared by the citrate-reduction method reported by Ferns. 50 mL 0.01% gold chloride trihydrate solution was boiled while continuously stirred and 0.5 mL OF 1% tri-sodium citrate solution was added rapidly. After

15 minutes of boiling, heating was stopped and was stirred for 1 h. The solution was then cooled and stored at 4º C.

Sample preparation: 50 µg of Cardiac Troponin I is first used to make a solution of 100 µL with concentration of 0.5 µg/µL. Gold nanoparticle conjugation is obtained by mixing cTnI solution AuNPs in 90:10 ratio. 10 µL of the cTnI solution is mixed with 90 µL of AuNPs and left overnight. cTnI concentration in the solution is calculated to be 0.05 µg/µL. The solution is further diluted by adding 20 µL of the solution to 480 µL of Phosphate buffer solution (PBS) and the final concentration of cTnI is 2 ng/µL. This solution is used to make sub-concentration solutions by mixing with PBS. Three samples were used with concentration of 2 ng/µL, 1 ng/µL, and 0.75 ng/µL.

The UV-Vis spectroscopy is carried out using spectrophotometer of Electronics India Limited, India. Range of the instrument was from 340 to 960 nm with resolution of 1 nm equipped with monochromator of 600 lines/mm holographic grating, and light source of 6V, 10W Tungsten Halogen lamp. FTIR spectroscopy is carried out using Thermo Nicolet iS5 FTIR spectrometer which had a spectral range of 7800-350 cm-1, mid-infrared KBr beam splitter, signal to noise ratio of 8000:1 (Peak to Peak) and spectral resolution of less than 0.8 cm-1, and wavelength precision of 0.01 cm-1 at 2000 cm-1. Detector of the system is fast recovery deuterated triglycine sulfate (DTGS) detector and temperature controlled solid-state Near-IR diode laser is used as Laser source.

Effectiveness of denoising method using wavelet transform depends on three parameters namely wavelet bases, decomposition level, and threshold method. The threshold method generally used in the wavelet transform are of two types: Hard and Soft threshold. In the hard

threshold method, the value of a detail coefficient less than the threshold value is set to zero and when it is above the threshold value, it remains the same.

$$w_\lambda = \begin{cases} w, & |w| \geq \lambda \\ 0, & |w| < \lambda \end{cases} \quad \text{(vii)}$$

On the other hand, in the soft threshold method, if the value of the detail coefficient is less than the threshold value, they are set to zero, but, if the value is above the threshold level, the absolute value of the threshold is subtracted from the wavelet coefficient.

$$w_\lambda = \begin{cases} [sign(w)](|w| - \lambda), & |w| \geq \lambda \\ 0, & |w| < \lambda \end{cases} \quad \text{(viii)}$$

Popular threshold selection rules for wavelet-based denoising includes universal threshold, SURE threshold, heuristic threshold, and minimax threshold. In the start, Donoho proposed fixed value thresholding to denoise signals calculated as:

$$\lambda = \sqrt{2ln\,(n)/n} \quad \text{(ix)}$$

where n is the number of wavelet coefficients [31]. Noise dependent threshold is then obtained by modifying the fixed value threshold known as the universal threshold. The universal threshold is calculated as:

$$\lambda = \sigma\sqrt{2ln\,(N)} \quad \text{(x)}$$

where N is the length of the noisy signal; σ is the standard deviation of noise estimated as:

$$\sigma = \frac{median(|Y_{ij}|)}{0.6745} \quad \text{(xi)}$$

where Y_{ij} are coefficient of decomposition level. We use the universal threshold selection rule for threshold calculation.

Denoising procedure of signal can be summarized as: -

1. Noisy signal models: - Signals under investigation are first imported in MATLAB and Gaussian white noise of different SNR values are added to it.

2. Decomposition level: - The level of decomposition is decided and the forward DD-DTCWT is calculated.
3. Threshold calculation: - The threshold value for each detail coefficient sub-band of the decomposed signal is estimated.
4. Threshold application: - Apply threshold value to detail coefficient of both tree, real and imaginary coefficients.
5. Reconstruction: - Inverse DD-DTCWT is applied to obtain the denoised signal.
6. Performance parameters: - To evaluate the capability of the denoising method, performance parameters are calculated

To verify the effectiveness of the proposed method, performance indicators are used. Signal to noise ratio (SNR) and root mean square error (RMSE) are used in this study. Mean square error is the average squared difference between the estimated value and the actual value. The square root of mean square error gives the RMSE calculated as:

$$RMSE = \sqrt{\frac{\sum_{i=1}^{N}(x_i - \tilde{x}_i)^2}{N}} \quad \text{(xii)}$$

where x_i is the original signal, $\tilde{x}_i$ is the reconstructed signal and N is the signal length. Another performance indicator considered here for evaluating the effectiveness of the method is SNR calculated in dB as the ratio of mean squared magnitude of the signal to the mean squared magnitude of the noise. SNR gives a qualitative analysis of the signal about the impact of noise on the signal calculated as:

$$SNR = 10 \times log\frac{\delta^2}{D} \quad \text{(xiii)}$$

where $\delta^2 = \frac{1}{N}\sum_{i=1}^{N}(x_i - \acute{x})^2$, $D = \frac{1}{N}\sum_{i=1}^{N}(x_i - \tilde{x}_i)^2$ and $\acute{x} = \frac{1}{N}\sum_{i=1}^{N} x_i$

5.3 Results and Discussion

5.3.1 Biomarker detection

Figure 5.2(a) shows TEM image of Gold Nanoparticles. The pure AuNPs have a uniform population of sphere-shaped particles with an average size of 10nm which is further verified by UV-Vis spectrophotometry shown in Figure 5.3(a). The synthesized nanoparticles then conjugated with cTnI. The cTnI-AuNP conjugates have an average size of 100nm as seen in Figure 5.2(b) due to large size of the protein.

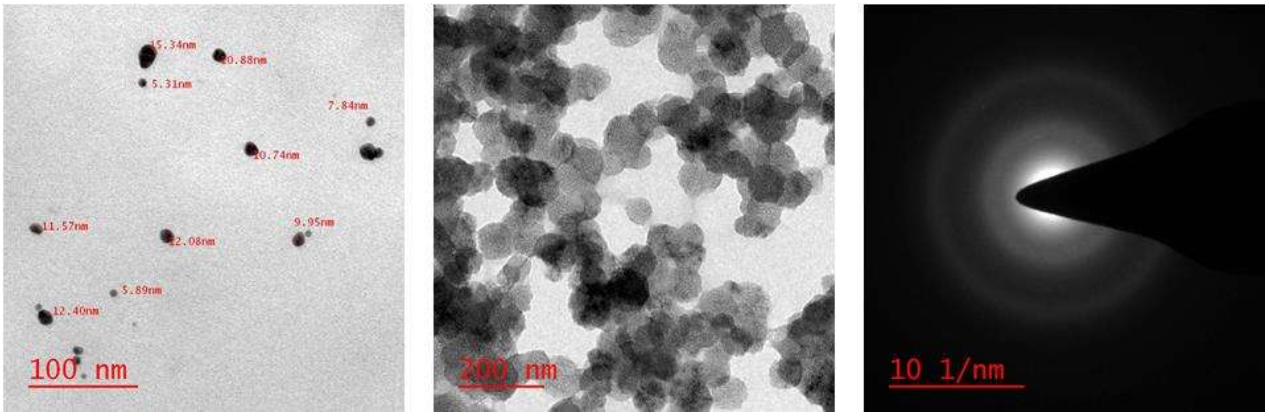

Figure 5.2: TEM Images of (a) Gold Nanoparticles (b) cTnI conjugated AuNPs and (c) SAD pattern

It is visible from the graph that synthesized nanoparticles have local surface plasmon resonance at 530 nm. Figure 5.3(b) shows the UV-Visible spectra of pure Gold nanoparticles and cTnI conjugated Gold nanoparticles. It can be observed from the spectra that the SPR maximum of the gold nanoparticles at around 530 nm is completely quenched. Although, it is extensively reported that 100nm pure or protein bind AuNP shows a peak at 570nm in UV-Visible spectra which should be the case with cTnI-GNP moiety. However, the absence of any visible peak in the spectra indicates the shielding effects by the protein molecule.

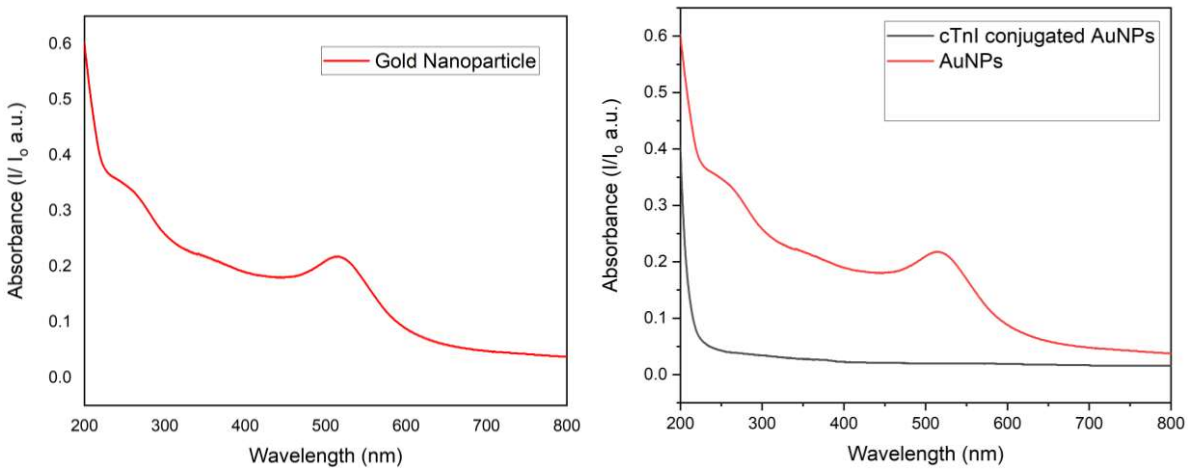

Figure 5.3: UV-Visible spectra (a) Gold Nanoparticles (b) Gold nano particles and cTnI conjugated Gold nanoparticles.

From above, it is clear that the conjugation of cTnI causes the quenching of the LSPR peak of the Gold nanoparticles. Further, to check the effect of concentration variation of cTnI, three different UV-Visible spectra were acquired for three different concentrations shown in figure 5.3(b). It can be observed from the spectra that cTnI conjugated AuNPs has a dominant peak at ~ 200 nm. Also, the main peak of cTnI conjugated AuNPs displays a clear monotonic dependence on cTnI concentration.

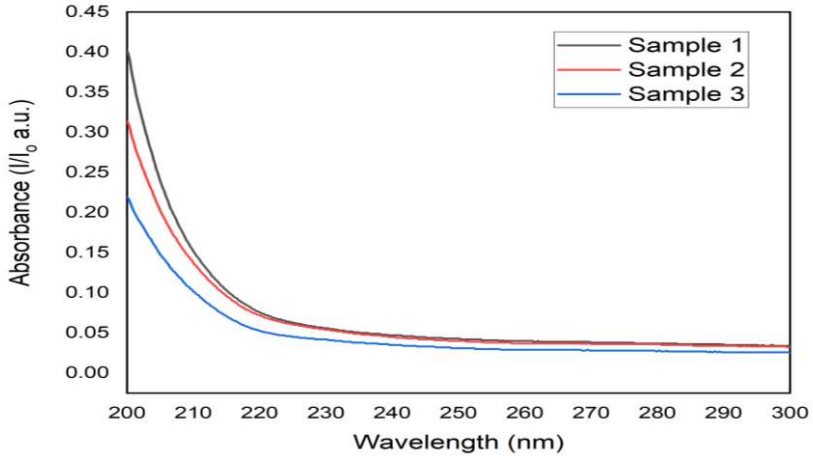

Figure 5.4: UV-Visible spectra of cTnI conjugated gold nanoparticles for three different concentrations.

Figure 5.5 shows FTIR spectrophotometry of cTnI conjugated gold nanoparticles for three different concentrations of cTnI. Dominant peaks in FTIR are at 3460 cm-1, 1650 cm-1, 1060 cm-

1, 560 cm-1, and a small peak at 1550 cm-1. As the concentration of the cTnI varies, the transmittance intensity for prominent peaks at 1650 cm-1, and 3460 cm-1 shows a linear variation.

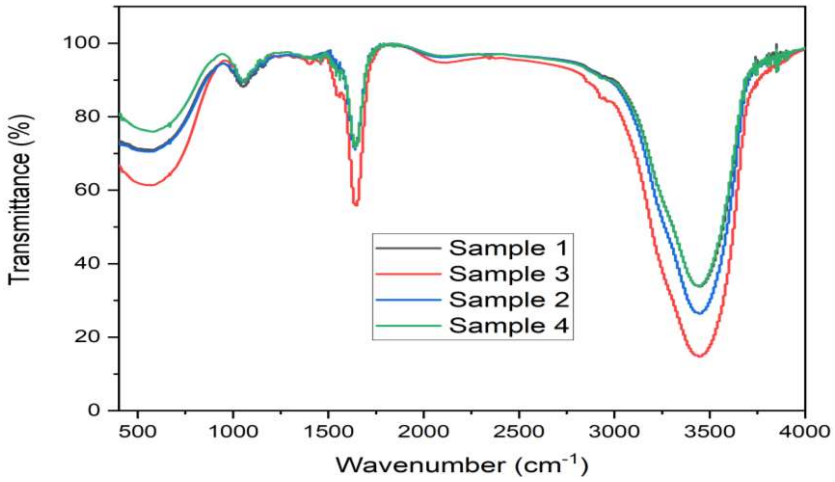

Figure 5.5: FTIR of Gold nanoparticle and cTnI conjugated gold nanoparticles

5.3.2 Spectroscopy Signal processing

5.3.2.1 Spike removal from signal

At first, we tried to evaluate the capability of wavelet transform to remove cosmic spikes by decomposing the signal to different levels so that simultaneous denoising can be carried out. This is explored using the Raman spectrum of Forsterite-Hydroxyapatite thin film on stainless steel. Raman spectra has intense Raman band at 880 cm-1(B4) and 906 cm-1 (B5) with low intensity Raman peaks at 129 cm-1 (B1), 300 cm-1(B2), 383 cm-1 (B3) and 962 cm-1 (B6). The spectrum exhibits four simulated spikes at 366 cm-1 (S1), 622 cm-1 (S2), 746 cm-1 (S3) and 1106 cm-1 (S4) cm-1 with varying intensity from 1.6 times of maximum intensity Raman band to 0.1 times of maximum intensity Raman band as shown in figure 5.6(a). Simulated signal wavelet decomposition was performed using DD-DTCWT. Ideally, for spike removal, it is required that the approximation coefficient possesses properties like reduction in Raman band intensity by the noise level, Raman band profile is preserved and spikes be removed.

From Figure 5.6(c), it is evident that desired properties were not obtained as spikes also appear in the approximate coefficient along with Raman bands. It can be concluded from the above observation that simultaneous spike removal while denoising is not possible. Figure 5.6(b) shows clear discrimination of spikes from Raman bands and noises that occurs within the detail coefficients especially at first level details. If spike location from first-level detail coefficients can be projected into the appropriate location of the original Raman signal, spike removal can be performed. In Fourier analysis, this process is not possible as time information is lost while time information is preserved in the wavelet transform. The additional argument of peak width while locating the spike location is applied in the time domain. It is observed that FWHM of the spike is generally near to 1cm-1 while for the Raman band, it is much higher. This allows removing any location selected from the first-level decomposition which corresponds to Raman bands. After the appropriate location of the spike, interpolation is applied to remove the spike. Figure 5.6(a) and 5.6(d) shows the simulated spiked signal and signal after removing spikes.

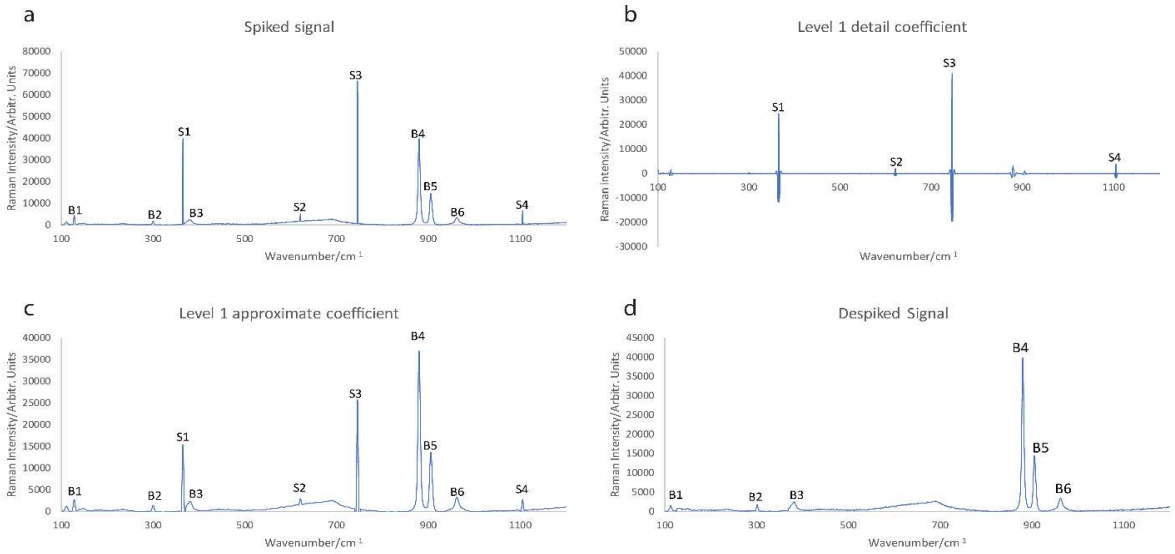

Figure 5.6. (a) Raman signal with simulated spikes (b) Level 1 detail coefficient of DDDTCWT (c)Level 1 approximate coefficient of Double Density dual-tree complex wavelet transforms (d) Despiked Raman signal

5.3.2.2 Denoising of Noisy spectrum model

First, the denoising is applied to standard signals: Block, Bump, HeaviSine and Doppler. Noisy signal models are obtained and denoised using DD-DTCWT, DT-CWT, DWT, Savitzky-Golay smoothing (3rd and 1st order). Table 5.1 shows performance parameters for different signals.

Table 5.1: - Signal to noise ratio and Root mean square error for test signals

	Block		Bump		HeaviSine		Doppler	
	SNR	RMSE	SNR	RMSE	SNR	RMSE	SNR	RMSE
Signal	15.06	0.1269	22.84	0.1777	24.54	0.1828	4.34	0.1778
DD-DTCWT	**19.28**	**0.0755**	**28.21**	**0.0956**	**32.43**	**0.0736**	**12.61**	**0.0691**
DT-CWT	18.36	0.0855	26.51	0.1165	30.56	0.0913	10.71	0.0884
DWT	14.45	0.1477	16.01	0.1119	29.66	0.1016	10.30	0.0930
SG3	15.40	0.1201	21.32	0.2116	28.91	0.1104	9.37	0.105
SG1	12.48	0.1606	19.61	0.2557	29.97	0.0977	11.1	0.083

* DD-DTCWT- Double density dual-tree complex wavelet transform, DT-CWT- Dual tree complex wavelet transform, DWT- Discrete wavelet transform, SG3-Savitzky-Golay 3rd order smoothing, SG1-Savitzky-Golay 1st order smoothing

The above results show the superiority of DD-DTCWT in denoising the test signals, but the application of a denoising method to Raman signal is difficult due to the presence of low-intensity peaks. A denoising method is said to be effective if it is capable to increase the signal to noise ratio (SNR) of the signal while retaining these small details. To study this, a pre-processed Raman signal of Glucose, Sucrose, and Xanthan is obtained from online available data bank and noisy signal models are simulated by adding white Gaussian noise of different levels as obtained for previous signals. Figure 5.7(a) and 5.7(b) shows the pre-processed Raman signal of Xanthan and Glucose. Figure 4(c) and 4(d) is noisy Raman signal models with SNR for noisy signals as 25.59 and 17.55 respectively and RMSE as 0.1814 and 0.1756 respectively. Denoising methods are applied and the denoised signal parameters are calculated and tabulated in table 5.2. Table 5.2

also has SNR and RMSE data for the Sucrose Raman signal. Figure 5.7(e) and 5.7(f) show the Raman signal denoised by applying the proposed method. It can be observed that DD-DTCWT can denoise the noisy Raman signal effectively while retaining small features.

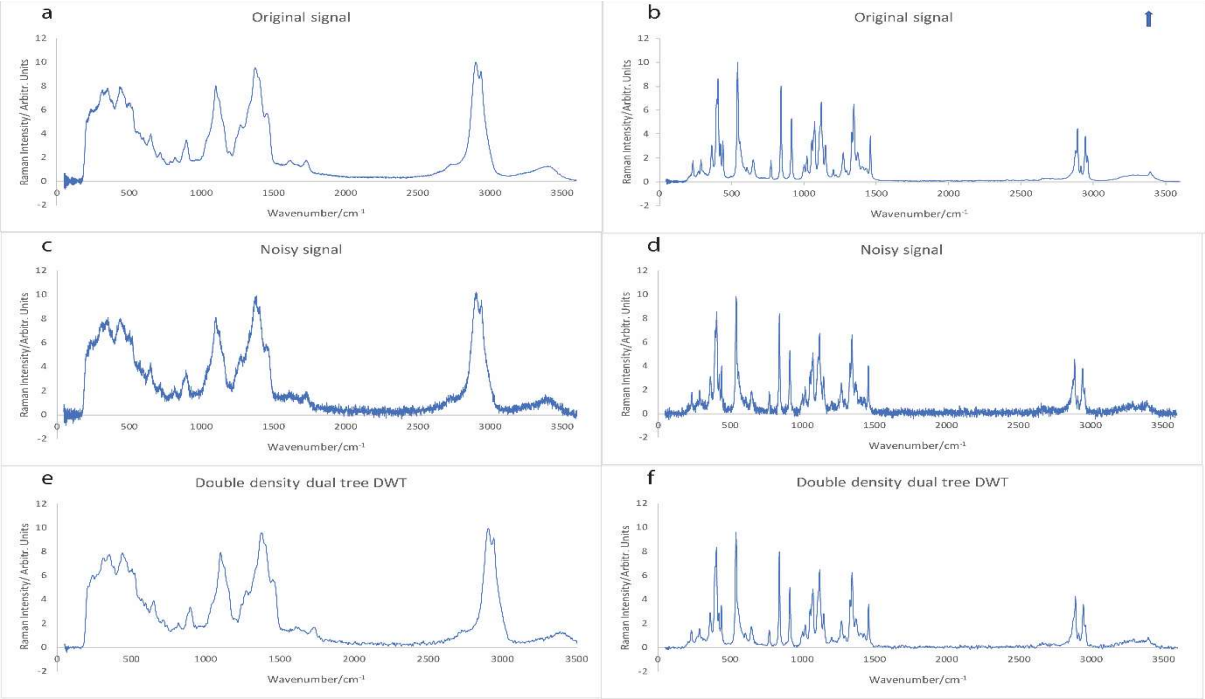

Figure 5.7. (a) Xanthan Raman Spectrum (b) Glucose Raman Spectrum (c) Xanthan Raman spectrum noise model (d) Glucose Raman spectrum noise model (e) Double Density dual-tree complex wavelet transform denoised Xanthan Raman spectrum (f) Double Density dual-tree complex wavelet transform denoised Glucose Raman spectrum

Figure 5.8(a) and 5.8(b) shows the variation of denoised signal SNR and RMSE using different methods as the noise level is varied. Here, it can be observed that for the high value of noise, both 1st order and 3rd order Savitsky-Golay works well but as the noise level decreases, 1st order Savitsky-Golay smoothing capability to denoise signal goes on decreasing as compared to 3rd order Savitsky-Golay smoothing. It can be concluded from these results that for denoising Raman signal using Savitsky-Golay smoothing, it is required to perform random adjustments of order and frame length of the smoothing method to obtain good results. Also, DWT denoising capability is better than the Savitsky-Golay method but SNR and RMSE are lesser than DD-

DTCWT. DD-DTCWT always gives better SNR and RMSE and is not affected by the noise level introduced to the signal from which it can be concluded that DD-DTCWT is a better method to denoise the Raman signal.

Table 5.2: - Signal to noise ratio and Root means square error for actual Raman signals

	Xanthan		Glucose		Sucrose	
	SNR	RMSE	SNR	RMSE	SNR	RMSE
Signal	25.5966	0.1814	17.5599	0.1756	18.7418	0.1794
DD-DTDWT	**32.6063**	**0.0809**	**24.5431**	**0.0781**	**25.1465**	**0.0854**
DT-DWT	30.8309	0.0993	23.3818	0.0899	24.5562	0.0920
DWT	30.3400	0.1051	22.3900	0.1007	23.5300	0.1035
SG3	29.3250	0.1182	21.9681	0.1059	23.2102	0.1075
SG1	30.5403	0.1027	23.0310	0.0927	23.6754	0.1011

* DD-DTCWT- Double density dual-tree complex wavelet transform, DT-CWT- Dual tree complex wavelet transform, DWT- Discrete wavelet transform, SG3-Savitzky-Golay 3rd order smoothing, SG1-Savitzky-Golay 1st order smoothing

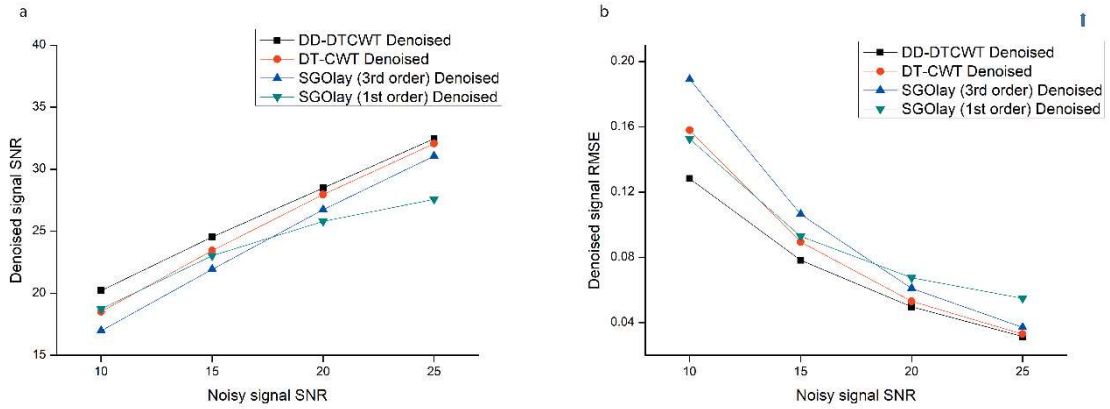

Figure 5.8. (a) Variation of Signal to noise ratio of the denoised signal using different methods as the noise level is varied (b) Variation of Root mean square error of the denoised signal using different methods as the noise level is varied

5.4 Conclusion

cTnI quantification by UV-Visible spectroscopy is a viable, safe and reliable method with very less difficulties. Instrumentation requirement for such analysis is low cost and portable and thus can be carried out easily in any lab or can be used as point-of care technique. The method

proposed here is suitable for cTnI at very low concentrations. UV-Visible spectra of gold nanoparticles had been found to show peak at ~530 nm conforming the formation of spherical gold nanoparticle with average diameter of 10 nm. The conjugation of the cTnI with gold nanoparticles is done carried out and UV-Visible spectra was recorded. It was found that the spectra of cTnI conjugated AuNPs doesn't had peak at 530 nm and a peak near 200 nm is observed whose intensity was found to be directly proportional to the concentration of the cTnI. Concentration variation of cTnI in gold nanoparticle solution is further verified by FTIR.

References

[1] Raman, C.V. and Krishnan, K.S., 1928. A new type of secondary radiation. *Nature*, *12* (3048), p.501.

[2] Banwell, C.N. and McCash, E.M., 1994. *Fundamentals of molecular spectroscopy* (Vol. 851). New York: McGraw-Hill.

[3] Haynes, C.L., McFarland, A.D. and Van Duyne, R.P., 2005. Surface-enhanced Raman spectroscopy.

[4] Bocklitz, T., Walter, A., Hartmann, K., Rösch, P. and Popp, J., 2011. How to pre-process Raman spectra for reliable and stable models?. *Analytica chimica acta*, *704*(1-2), pp.47-56.

[5] Braz, A., López-López, M. and García-Ruiz, C., 2013. Raman spectroscopy for forensic analysis of inks in questioned documents. *Forensic science international*, *232*(1-3), pp.206-212.

[6] McCreery, R.L., 2005. *Raman spectroscopy for chemical analysis* (Vol. 225). John Wiley & Sons.

[7] Harz, M., Kiehntopf, M., Stöckel, S., Rösch, P., Straube, E., Deufel, T. and Popp, J., 2009. Direct analysis of clinical relevant single bacterial cells from cerebrospinal fluid during

bacterial meningitis by means of micro-Raman spectroscopy. *Journal of biophotonics*, *2*(1-2), pp.70-80.

[8] Vankeirsbilck, T., Vercauteren, A., Baeyens, W., Van der Weken, G., Verpoort, F., Vergote, G. and Remon, J.P., 2002. Applications of Raman spectroscopy in pharmaceutical analysis. *TrAC trends in analytical chemistry*, *21*(12), pp.869-877.

[9] Muehlethaler, C., Leona, M. and Lombardi, J.R., 2015. Review of surface enhanced Raman scattering applications in forensic science. *Analytical chemistry*, *88*(1), pp.152-169.

[10] Smulko, J., Wróbel, M.S. and Barman, I., 2015, June. Noise in biological Raman spectroscopy. In *2015 International Conference on Noise and Fluctuations (ICNF)* (pp. 1-6). IEEE.

[11] Barton, S.J., Ward, T.E. and Hennelly, B.M., 2018. Algorithm for optimal denoising of Raman spectra. *Analytical Methods*, *10*(30), pp.3759-3769.

[12] Li, G., 2008, December. Noise removal of Raman spectra using interval thresholding method. In *2008 Second International Symposium on Intelligent Information Technology Application* (Vol. 1, pp. 535-539). IEEE.

[13] Liu, H., Zhang, Z., Liu, S., Yan, L., Liu, T. and Zhang, T., 2015. Joint baseline-correction and denoising for Raman spectra. *Applied spectroscopy*, *69*(9), pp.1013-1022.

[14] Chen, S., Lin, X., Yuen, C., Padmanabhan, S., Beuerman, R.W. and Liu, Q., 2014. Recovery of Raman spectra with low signal-to-noise ratio using Wiener estimation. *Optics express*, *22*(10), pp.12102-12114.

[15] Smulko, J. and Wróbel, M.S., 2017, March. Noise sources in Raman spectroscopy of biological objects. In *Dynamics and Fluctuations in Biomedical Photonics XIV* (Vol. 10063, p. 100630Q). International Society for Optics and Photonics.

[16] Barnes, R.J., Dhanoa, M.S. and Lister, S.J., 1989. Standard normal variate transformation and de-trending of near-infrared diffuse reflectance spectra. *Applied spectroscopy*, *43*(5), pp.772-777.

[17] Ramos, P.M. and Ruisánchez, I., 2005. Noise and background removal in Raman spectra of ancient pigments using wavelet transform. *Journal of Raman Spectroscopy: An International Journal for Original Work in all Aspects of Raman Spectroscopy, Including Higher Order Processes, and also Brillouin and Rayleigh Scattering*, *36*(9), pp.848-856.

[18] Hu, Y., Jiang, T., Shen, A., Li, W., Wang, X. and Hu, J., 2007. A background elimination method based on wavelet transform for Raman spectra. *Chemometrics and Intelligent Laboratory Systems*, *85*(1), pp.94-101.

[19] Zhang, Z.M., Chen, S., Liang, Y.Z., Liu, Z.X., Zhang, Q.M., Ding, L.X., Ye, F. and Zhou, H., 2010. An intelligent background-correction algorithm for highly fluorescent samples in Raman spectroscopy. *Journal of Raman Spectroscopy*, *41*(6), pp.659-669.

[20] Beier, B.D. and Berger, A.J., 2009. Method for automated background subtraction from Raman spectra containing known contaminants. *Analyst*, *134*(6), pp.1198-1202.

[21] Kwiatkowski, A., Gnyba, M., Smulko, J. and Wierzba, P., 2010. Algorithms of chemicals detection using Raman spectra. *Metrology and Measurement Systems*, *17*(4), pp.549-559.

[22] Savitzky, A. and Golay, M.J., 1964. Smoothing and differentiation of data by simplified least squares procedures. *Analytical chemistry*, *36*(8), pp.1627-1639.

[23] Ehrentreich, F. and Sümmchen, L., 2001. Spike removal and denoising of Raman spectra by wavelet transform methods. *Analytical chemistry*, *73*(17), pp.4364-4373.

[24] Chen, H., Xu, W., Broderick, N. and Han, J., 2018. An adaptive denoising method for Raman spectroscopy based on lifting wavelet transform. *Journal of Raman Spectroscopy*, *49*(9), pp.1529-1539.

[25] Jaffe AS, Babuin L, Apple FS. Biomarkers in Acute Cardiac Disease. Journal of the American College of Cardiology 2006;48:1–11. https://doi.org/10.1016/j.jacc.2006.02.056.

[26] Danese E, Montagnana M. An historical approach to the diagnostic biomarkers of acute coronary syndrome. Annals of Translational Medicine 2016;4:194–194. https://doi.org/10.21037/atm.2016.05.19.

[27] Agarwal DK, Kandpal M, Surya SG. Characterization and detection of cardiac Troponin-T protein by using 'aptamer' mediated biofunctionalization of ZnO thin-film transistor. Applied Surface Science 2019;466:874–81. https://doi.org/10.1016/j.apsusc.2018.10.086.

[28] Ahammad AJS, Choi Y-H, Koh K, Kim J-H, Lee J-J, Lee M. Electrochemical Detection of Cardiac Biomarker Troponin I at Gold Nanoparticle-Modified ITO Electrode by Using Open Circuit Potential. Int J Electrochem Sci 2011;6:11.

[29] Centi S, Bonel Sanmartin L, Tombelli S, Palchetti I, Mascini M. Detection of C Reactive Protein (CRP) in Serum by an Electrochemical Aptamer-Based Sandwich Assay. Electroanalysis 2009;21:1309–15. https://doi.org/10.1002/elan.200804560.

[30] Das G, Mecarini F, De Angelis F, Prasciolu M, Liberale C, Patrini M, et al. Attomole (amol) myoglobin Raman detection from plasmonic nanostructures. Microelectronic Engineering 2008;85:1282–5. https://doi.org/10.1016/j.mee.2007.12.082.

Part - III

USING
LEARNING-BASED APPROACH
FOR
CARDIAC MRI PROCESSING